

This discussion paper is/has been under review for the journal Biogeosciences (BG).
Please refer to the corresponding final paper in BG if available.

**Methane oxidation in
permeable sediments
at hydrocarbon seeps**

T. Treude and W. Ziebis

Methane oxidation in permeable sediments at hydrocarbon seeps in the Santa Barbara Channel, California

T. Treude^{1,*} and W. Ziebis¹

¹University of Southern California, Department of Marine Environmental Biology, Los Angeles,
CA, USA

*present address: Leibniz Institute of Marine Sciences (IFM-GEOMAR), Kiel, Germany

Received: 3 March 2010 – Accepted: 6 March 2010 – Published: 17 March 2010

Correspondence to: T. Treude (ttreude@ifm-geomar.de)

Published by Copernicus Publications on behalf of the European Geosciences Union.

Title Page

Abstract

Introduction

Conclusions

References

Tables

Figures

◀

▶

◀

▶

Back

Close

Full Screen / Esc

Printer-friendly Version

Interactive Discussion



Abstract

A shallow-water area in the Santa Barbara Channel (California), known collectively as the Coal Oil Point seep field, is one the largest natural submarine oil and gas emission areas in the world. Both gas and oil are seeping constantly through a predominantly sandy seabed into the ocean. This study focused on the methanotrophic activity within the surface sediments (0–15 cm) of the permeable seabed in the so-called Brian Seep area at a water depth ~ 10 m. Detailed investigations of biogeochemical parameters in the sediment surrounding active gas vents indicated that methane seepage through the permeable seabed induces a convective transport of fluids within the surface sediment layer, which results in a deeper penetration of oxidants (oxygen, sulfate) into the sediment, as well as in a faster removal of potentially inhibiting reduced end products (e.g. hydrogen sulfide). Methanotrophic activity was often found close to the sediment-water interface, indicating the involvement of aerobic bacteria. However, biogeochemical data suggests that the majority of methane is consumed by anaerobic oxidation of methane (AOM) coupled to sulfate reduction below the surface layer (> 15 cm), where sulfate is still available in high concentrations. This subsurface maximum of AOM activity in permeable sands is in contrast to known deep-sea seep habitats, where upward fluid advection through more fine-grained sediments leads to an accumulation of AOM activity within the top 10 cm of the sediments, because sulfate is rapidly depleted.

1 Introduction

Coal Oil Point seep field, an area of natural oil and gas seepage in the Santa Barbara Channel, California, is one the largest submarine natural oil and gas emission areas in the world (Allen and Mikolaj, 1970). Hydrocarbons are leaking from an oil reservoir ~ 1500 m below the seafloor and seeps occur along fractures in shallow water from the shoreline to 60 m water depths, in an area of about 18 km^2 . Both natural gas and oil are seeping constantly through a predominantly sandy seabed into the ocean

BGD

7, 1905–1933, 2010

Methane oxidation in permeable sediments at hydrocarbon seeps

T. Treude and W. Ziebis

Title Page

Abstract

Introduction

Conclusions

References

Tables

Figures

◀

▶

◀

▶

Back

Close

Full Screen / Esc

Printer-friendly Version

Interactive Discussion



at estimated flux rates of $1.7 \times 10^5 \text{ m}^3 \text{ d}^{-1}$ of hydrocarbon gases (88% methane) and $1.6 \times 10^4 \text{ L d}^{-1}$ of crude oil (~ 100 barrels a day) (Hornafius et al., 1999). The intensity of seepage is variable and may be linked to tidal changes or seismic activity (Boles and Clark, 2001). Methane plumes in the water column have been observed in an area of $\sim 70 \text{ km}^2$ with emission rates of $5 \times 10^4 \text{ mol CH}_4 \text{ d}^{-1}$. This methane flux into the atmospheres is estimated to account for approximately 1% of the total methane export across the sediment-water interface (Mau et al., 2007). The remaining 99% of methane that are emitted from the sediments are assumed to be consumed by methanotrophic bacteria in surface sediments or in the water column.

The present study focused on methanotrophic activity and biogeochemical parameters within the sediments of a study area known as “Brian Seep”, which is located off the coast of Coal Oil Point at water depths around 10 m (Kinnaman et al., 2010; Kinnaman et al., 2007). In this coastal area, sediments consist of permeable sand (permeability $\sim 10^{-11} \text{ m}^2$, see results) allowing a faster advective transport of fluids and gases through the sediment matrix compared to fine-grained cohesive clays found in benthic environments of the deeper oceans (Huettel et al., 1998, 2003; Ziebis et al., 1996b). In addition, water movements induced by waves and tidal currents constantly reshape the sediment surface topography, which should enable fast mixing rates between sediment porewater and overlying water column (Precht et al., 2004). It was the aim of the present study to investigate how gas venting through the dynamic permeable seabed impacts aerobic and anaerobic microbial methane oxidation. Since both processes are controlled by the supply of their electron acceptors, i.e., oxygen and sulfate, respectively (Nauhaus et al., 2002; Treude, 2003; Niemann et al., 2006), we expected to find differences in their vertical distribution in this coastal area when compared to less permeable fine-grained sediments that dominate deep-sea seep habitats. Our data indicate that gas venting at Brian Seep results in convective porewater transport processes resulting in a thin surface layer of aerobic methanotrophy and a much deeper zone of anaerobic oxidation of methane (AOM).

Methane oxidation in permeable sediments at hydrocarbon seeps

T. Treude and W. Ziebis

Title Page

Abstract

Introduction

Conclusions

References

Tables

Figures

◀

▶

◀

▶

Back

Close

Full Screen / Esc

Printer-friendly Version

Interactive Discussion



2 Materials and methods

2.1 Sediment sampling

Sediments samples were taken by SCUBA diving at Brian Seep (34°24.109' N, 119°49.917' W, water depth 10 m) using two sizes of polycarbonate core liners (inner diameter/total length: 5.4/40 and 2.5/30 cm, respectively). Core liners were forced into the sediment using rubber mallets. In general, not more than ~15 cm sediment cores could be retrieved, because the sandy surface coverage was followed by a coarse gravel bed impeding a deeper penetration of the core liners. Samples were taken in April, June and November of 2006. In April, a horizontal transect was sampled at 0, 20, 50, 100, 200, and 400 cm distances from a gas vent in the Brian Seep area featuring a continuous release of gas, which was visible as streams of bubbles (methane content ~90%, Kinnaman et al., 2010). At a distance of 400 cm, gas bubbles also emerged from the sediment, after core liners were forced into the sediment. In June, samples were taken at two different gas vents within the Brian Seep area which were approximately 20 m apart. Cores were taken as close to the central gas venting conduits as possible. In November samples were taken along a shorter transect at 0, 20, 40, and 60 cm distances away from another gas vent in the Brian Seep area. Water temperatures in the seep area varied between 11, 14, and 15°C in April, June and November 2006, respectively (NOAA National Data Buoy Center, Station 46045). Immediately after retrieval, sediment cores were transported to the laboratory for further processing. In the following, the sampling locations will be abbreviated with the distance in cm followed by the initial of the month for April and November, for example: 0-cm-A and 20-cm-N. For the June sampling the two vents that were sampled will be called Vent A and Vent B.

BGD

7, 1905–1933, 2010

Methane oxidation in permeable sediments at hydrocarbon seeps

T. Treude and W. Ziebis

Title Page

Abstract

Introduction

Conclusions

References

Tables

Figures

◀

▶

◀

▶

Back

Close

Full Screen / Esc

Printer-friendly Version

Interactive Discussion



2.2 Microprofiling

Oxygen, H₂S and pH microgradients were measured with microelectrodes at room temperature (19 °C) in intact large cores (i.d. 5.4 cm) immediately after retrieval. The oxygen sensors were Clark-type amperometric electrodes with a built-in reference and a guard cathode (Unisense OX50; Revsbech, 1989) with a tip diameter of 50 μm, a stirring sensitivity of 1% and a 90% response time <1 s. The electrode currents have a linear response to oxygen dissolved in water. A two-point calibration was performed by inserting the oxygen electrode into a calibration chamber filled with water from the sampling site, which was purged with air (100% saturation) or nitrogen (0% saturation) at the in situ temperature. The H₂S microsensor used in the analysis was a miniaturized amperometric sensor with an internal reference and a guard electrode (Unisense H2S25; Jeroschewsky et al., 1996; Kühl et al., 1998). The sensor had a long (5 cm) tapered tip with a tip diameter of 50 μm. The response time was <2 s. Total sulfide concentrations (that is here the total sum $\Sigma\text{H}_2\text{S}=[\text{H}_2\text{S}]+[\text{HS}^-]+[\text{S}_2^{2-}]$, where square brackets denote concentration) were calculated using pH values measured in tandem with the H₂S profiles using long needle combination electrodes (Diamond General), which were connected to a high-impedance mV-meter (Unisense PHM210). Calibration of the H₂S microsensor was performed with Na₂S standards of known concentrations measured by colorimetric analysis (Cline, 1969). The pH electrode was calibrated using standard pH buffer solutions (VWR). The electrodes were attached to a micromanipulator and moved vertically into the sediment via a computer-controlled motor (Unisense MC18011). Amperometric sensors were connected to a high-sensitivity picoammeter (Unisense PA2000) and the cathodes were polarized against an internal reference.

2.3 Whole sediment sampling

Sediment samples for the determination of methane concentration (ex-situ determination), porosity, density, grain size, permeability, and fluorescence in situ hybridization (FISH) were taken with large core liners (i.d. 5.4 cm) and sectioned in 1-cm-intervals.

BGD

7, 1905–1933, 2010

Methane oxidation in permeable sediments at hydrocarbon seeps

T. Treude and W. Ziebis

Title Page

Abstract

Introduction

Conclusions

References

Tables

Figures

◀

▶

◀

▶

Back

Close

Full Screen / Esc

Printer-friendly Version

Interactive Discussion



For the analysis of methane, five cm³ sediment were taken with cut-off syringes and transferred into 60 ml glass vials filled with 35 ml sodium hydroxide (2.5% w/w). The vials were closed quickly with butyl rubber stoppers, sealed with aluminum crimps, and shaken thoroughly to equilibrate the pore water methane into the headspace.

Methane concentrations were determined by injection of 200 µl headspace into a gas chromatograph (Shimadzu, Model 2014) equipped with a packed stainless steel Supelco Custom Column (50/50 mixture, 80/100 Porapak N support, 80/100 Porapak Q column, 6 ft × 1/8 in) and a flame ionization detector. The carrier gas was helium at a flow rate of 30 ml min⁻¹. The column temperature was 60 °C. Carbon isotope ratios of methane were determined with inline ratio monitoring mass spectrometry as described by Rice et al. (2001). For porosity and density determination, approximately five cm³ sediment were transferred into pre-weighed 15 ml plastic centrifuge vials with a volume scale bar and closed with a plastic screw cap. The vials were centrifuged (2200 g, 10 min), weighed, filled with water to a defined volume, weighed again, dried and weighed a third time. Density was calculated by dividing the sediment wet weight by the sediment volume (sediment volume with added water minus volume of added water). Porosity was calculated by dividing the pore water volume (wet weight minus dry weight) by the sediment volume. For the determination of grain size and permeability the dried sediment was finally sieved through different mesh sizes (1000, 500, 250, and 125 µm) and weighed. Percentages of grain sizes were determined from weight ratios. Permeability of the sediment was calculated according to Krumbein and Monk (1943). For FISH analyses 0.5 cm³ of each sediment slice were transferred into 1.5 ml formaldehyde (final concentration 3%) and fixed for 2–4 h. After fixation, the sample was washed twice with 1 × PBS (10 mmol L⁻¹ sodium phosphate, 130 mmol L⁻¹ NaCl) and finally stored in 1 × PBS/EtOH (1:1) at –25 °C.

BGD

7, 1905–1933, 2010

Methane oxidation in permeable sediments at hydrocarbon seeps

T. Treude and W. Ziebis

Title Page

Abstract

Introduction

Conclusions

References

Tables

Figures

◀

▶

◀

▶

Back

Close

Full Screen / Esc

Printer-friendly Version

Interactive Discussion



2.4 Porewater extraction and analyses

Porewater samples from sandy sediment cores are difficult to extract by normal sediment processing of core slicing and porewater pressing. It is best to obtain porewater samples from intact cores as well as simultaneously from all depth to avoid porewater circulation and thus artifacts in the porewater data. We used a porewater extraction device designed for sandy sediments (Ziebis, unpublished). The cores were taken with core liners (i.d. 5.4 cm) that were perforated with lines of silicon-filled holes in 2-cm vertical intervals on opposite sides and alternating depth, to allow a depth resolution of 1 cm. The core was held in place so that double-sided needles that were mounted horizontally on sliding racks to both sides of the core could be pushed towards the core so that all the needles at all depth penetrated into the sediment. The other side of the needles was sealed with a rubber membrane. Vacutainers that were also mounted horizontally in racks to both sides were pushed onto the needles, so that the membrane was pushed aside and the needle penetrated through the stopper. By the underpressure in the vacutainers, porewater was drawn simultaneously from all depth intervals. Although this principle worked well to obtain undisturbed samples for pore water analyses, sometimes, needles were clogged and porewater profiles were incomplete.

The gained porewater was subsampled for the analyses of sulfate and ammonium concentrations. For sulfate concentration, one ml porewater was transferred into one ml zinc acetate (5% w/w). Porewater sulfate concentrations were measured using nonsuppressed ion chromatography with an autosampler (Spark Holland Basic and Marathon, injection volume 50 μ l), an anion exchange column (LCA A14, Sykam) and a conductivity detector (S3110, Sykam). Ammonium concentrations in the porewater were determined via conductivity by the flow-injection method for small sample volumes developed by Hall and Aller (1992).

BGD

7, 1905–1933, 2010

Methane oxidation in permeable sediments at hydrocarbon seeps

T. Treude and W. Ziebis

Title Page

Abstract

Introduction

Conclusions

References

Tables

Figures

◀

▶

◀

▶

Back

Close

Full Screen / Esc

Printer-friendly Version

Interactive Discussion



2.5 Turnover rate measurements

Sediments for radiotracer incubation experiments were sampled with small core liners (i.d. 2.5 cm). At each distance along the transects (April, November) and at each vent (June) two to four replicates were taken for methane oxidation and sulfate reduction measurements, respectively. Radioactive tracers (1.5 kBq $^{14}\text{CH}_4$ dissolved in 15 μl water for methane oxidation, 200 KBq $^{35}\text{SO}_4$ dissolved in 6 μl water for sulfate reduction) were injected into the cores in 1-cm-intervals according to the whole-core injection method (Jørgensen, 1978). The cores were incubated at 10 °C for 24 h in the dark. After incubation, reactions were stopped by fixing 1 cm-sections in 2.5% sodium hydroxide (methane oxidation) and 20% zinc acetate (sulfate reduction). Control samples were first fixed before tracer addition. Methane oxidation (MOX) rates were determined by gas chromatography (total methane concentration), $^{14}\text{CH}_4$ combustion and $^{14}\text{CO}_2$ acidification as described in detail by Treude et al. (2005b). Sulfate reduction rates were determined according to the cold-chromium distillation method described by Kallmeyer et al. (2004).

2.6 Identification of anaerobic methane-oxidizing (ANME) organisms by fluorescence in situ hybridization (FISH)

Fixed samples were diluted (1:10) with PBS and treated by mild sonication for 20 s with a Branson probe (rod: Model 102, sonifier: Model 250) at an amplitude of 42 μm < 10 W. An aliquot (40 μl) was filtered on 0.2 μm GTTP polycarbonate filters (Millipore Isopore Membrane Filters). The filters were embedded in low gelling point agarose. Hybridization and staining with 4',6'-diamidino-2-phenylindole (DAPI) was performed as described previously (Snaidr et al., 1997). Mean values of ANME cell aggregate numbers were calculated by using ~70 randomly chosen grids for each filter section, corresponding to 100–500 hybridized cells. ALEXA 488-monolabeled oligonucleotides were purchased from Integrated DNA Technologies IDT DNA, San Diego, California. Probes and formamide (FA) concentrations used in this study were as fol-

BGD

7, 1905–1933, 2010

Methane oxidation in permeable sediments at hydrocarbon seeps

T. Treude and W. Ziebis

Title Page

Abstract

Introduction

Conclusions

References

Tables

Figures

◀

▶

◀

▶

Back

Close

Full Screen / Esc

Printer-friendly Version

Interactive Discussion



lows: ANME-1-350 targeting ANME-1 (Boetius et al., 2000), 40% FA), ANME-2-538 targeting ANME-2 (Treude et al., 2005a), 50% FA), ANME-3-1249 targeting ANME-3 (Niemann et al., 2006, 20% FA). To avoid background signals 10% Blocking Reagent (Roche) was added to hybridization buffers (20% vol/vol).

3 Results

3.1 April sampling, 0–400 cm transect

Data sets were available from 20-cm-A, 200-cm-A, and 400cm-A only (Fig. 1). Sediment cores were not included for the analyses when there was any evidence of pore-water leakage and thus indicating mixing of porewater within the core. Leakage often resulted for example from larger sand grains that were caught between the rubber stoppers and core liners (see also missing parameters at 20-cm-A and 200-cm-A). In the following, parameters will be described for each distance along the transect.

At 20-cm-A, oxygen penetration into the sediment was 8 mm with an almost straight profile from the sediment-water interface down to 6 mm, suggesting fluid transport other than diffusion (Fig. 1a). Oxygen concentration in the overlying bottom water was 140 μM , i.e., lower than that at 400-cm-A (200 μM Fig. 1j), which could be explained by oxygen consumption while the core was stored for ~ 1 h (the 20-cm-A core was profiled after the 400-cm-A core). Porewater sulfate concentrations at 20-cm-A did not change with depth staying at ~ 27 mM (Fig. 1b). The methane profile from the methane oxidation (MOX) core showed a subsurface maximum between 3 and 6 cm depth of max. 0.15 mM (Fig. 1d), which also coincided approximately with highest MOX rates (max. 82 $\text{nmol cm}^{-3} \text{d}^{-2}$, Fig. 1e) and a peak in sulfide concentration (max. 2.7 mM, Fig. 1c).

At 200-cm-A, sulfate reduction was between 10 and 50% of the measured MOX rates (5–47 $\text{nmol cm}^{-3} \text{d}^{-1}$ compared to 36–118 $\text{nmol cm}^{-3} \text{d}^{-1}$, Fig. 1i and h, respectively). Both activities were relatively evenly distributed over depth. Concentration and carbon isotopic values of methane revealed no clear trends ranging around 0.1 mM (ex-situ

Title Page

Abstract

Introduction

Conclusions

References

Tables

Figures

◀

▶

◀

▶

Back

Close

Full Screen / Esc

Printer-friendly Version

Interactive Discussion



methane core) and 0.05 mM (MOX core) (Fig. 1g) respectively -55‰ $\delta^{13}\text{C}$ (Fig. 1f).

At 400-cm-A oxygen continuously decreased with depth to $0\ \mu\text{M}$ at $\sim 8\ \text{mm}$, exhibiting a profile typical for diffusive transport (Fig. 1j). Sulfate showed little change except for a subsurface decrease to $\sim 20\ \text{mM}$ at 3 cm (Fig. 1k). Methane concentrations were low in the upper 4 cm ($\sim 0.02\ \text{mM}$ in ex-situ cores and $\sim 0.07\ \text{mM}$ in MOX cores) but increased with depth to max. 0.15 and 0.25 mM, respectively (Fig. 1n). Methane isotopic signatures showed a nearly linear depletion of the lighter carbon isotope with depth (Fig. 1m). The increasing heavier $\delta^{13}\text{C}$ value (-53.6‰ on top, -29.5‰ at the bottom) of the pore water methane suggests methane oxidation, which leaves the residual methane in the pore water enriched in the heavier carbon isotope. This was confirmed by the MOX rates, which were also low in the top 4 cm but then increased to max. $281\ \text{nmol cm}^{-3}\ \text{d}^{-1}$ with depth (Fig. 1o). Similarly, sulfide concentrations increased to $\sim 1.5\ \text{mM}$ (Fig. 1l), and sulfate reduction to max. $200\ \text{nmol cm}^{-3}\ \text{d}^{-1}$ below 4 cm depth (Fig. 1p). Porosity and permeability data are available only from 400-cm-A and revealed no clear trend over depth with values in the range of 0.30 to 0.36 and 9.6×10^{-12} to $6.9 \times 10^{-11}\ \text{m}^2$, respectively (data not shown).

In summary, methane concentrations were generally low over the entire transect, reaching maximum values of only 0.25 mM, which is below the expected saturation limit (between 1.48 and 1.36 mM at atmospheric pressure for the respective in-situ temperature, Yamamoto et al., 1976). There was an obvious difference in the distribution of microbial activity with distance from the vent. Close to the center there appeared to be a near-surface peak of activity around 4–5 cm. At a distance of 200 cm, activity was more or less evenly distributed over the core. At a distance of 400 cm most of the activity was located below 4 cm depth. Oxygen penetrated 8 mm into the sediment; hence, MOX activity at 0–1 cm sediment depth could potentially be attributed to aerobic methane oxidation, whereas MOX in deeper, anoxic layers was most likely anaerobic oxidation of methane (AOM). Consequently, sulfate reduction at 0–1 cm was probably coupled to organic matter degradation. Deeper sediment layers could be mixtures of both, sulfate reduction coupled to organic matter degradation as well as AOM. Areal rates of

Methane oxidation in permeable sediments at hydrocarbon seeps

T. Treude and W. Ziebis

Title Page

Abstract

Introduction

Conclusions

References

Tables

Figures

◀

▶

◀

▶

Back

Close

Full Screen / Esc

Printer-friendly Version

Interactive Discussion



MOX (including both aerobic and anaerobic processes) integrated over the top 10 cm sediment increased with distance from the vent to a maximum of $8.69 \text{ mmol}^{-2} \text{ d}^{-1}$ at 400-cm-A (Table 1). Areal rates of sulfate reduction were approximately half (1.67 and $4.08 \text{ mmol}^{-2} \text{ d}^{-1}$ at 20- and 400-cm-A, respectively) of the areal MOX (Table 1).

5 3.2 November sampling, 0–60 cm transect

Methane concentrations, $\delta^{13}\text{C}$ -values of methane, methane oxidation, sulfate reduction and ammonium concentrations from the 0–60 cm transect were plotted in 2-D-contour maps as a function of transect distance (x-axes) and sediment depth (y-axes) using the contouring software Surfer™ (gridding method “nearest neighbor”, Fig. 2). In the following, 2-D-patterns of each parameter within the transect will be described.

Methane concentrations revealed similar pattern in ex-situ (0–6 cm) and MOX-cores (0–8 cm) (Fig. 2a, b). Values generally increased from top ($\sim 0.03 \text{ mM}$) to bottom (max. 0.2 mM) of the cores indicating methane oxidation. Concentrations in the porewater remained always undersaturated (see above). Peaks in methane concentrations were identified at 0-cm-N (0.20 mM at 4–7 cm), 20-cm-N (0.17 mM at 7–8 cm), 40-cm-N (1.1 mM at 9–10 cm), and 60-cm-N (0.6 mM at 9–10 cm), respectively.

Carbon isotopic signatures of methane ($\delta^{13}\text{C}$, 0–6 cm) ranged between values of -54 to -38‰ (Fig. 2c). By trend, values increased with depth at 0-, 20-, and 40-cm-N (-54‰ at top and -38‰ at the bottom) indicating methane oxidation. In contrast, values at 60-cm-N became increasingly lighter (-43‰ at top and -54‰ at bottom).

MOX rates (0–8 cm) were highest in the top (0–1 cm) layer of most cores reaching average values of 66 , 34 , and $59 \text{ nmol cm}^{-3} \text{ d}^{-1}$ at 0-, 20-, and 40-cm-N, respectively (Fig. 2d). Rates decreased with depth to levels between 1 and $5 \text{ nmol cm}^{-3} \text{ d}^{-1}$. Two exceptions were 0-cm-N, where a second peak of $20 \text{ nmol cm}^{-3} \text{ d}^{-1}$ was found between 4 and 5 cm depth (Fig. 2d) and 60-cm-N, where MOX reached values of 27 and $50 \text{ nmol cm}^{-3} \text{ d}^{-1}$ at 9–10 and 10–11 cm depth, respectively. Areal MOX rates integrated over the top 10 were highest at 0-cm-N and lowest at 60-cm-N (1.34 and $0.61 \text{ mmol m}^{-2} \text{ d}^{-1}$, respectively, Table 1).

Title Page

Abstract

Introduction

Conclusions

References

Tables

Figures

◀

▶

◀

▶

Back

Close

Full Screen / Esc

Printer-friendly Version

Interactive Discussion



Methane oxidation in permeable sediments at hydrocarbon seeps

T. Treude and W. Ziebis

Title Page

Abstract

Introduction

Conclusions

References

Tables

Figures

◀

▶

◀

▶

Back

Close

Full Screen / Esc

Printer-friendly Version

Interactive Discussion



Sulfate reduction rates (0–10 cm) generally revealed highest rates at the topmost layer ($\sim 25 \text{ nmol cm}^{-3} \text{ d}^{-1}$, Fig. 2f) and lowest rates at the bottom ($< 10 \text{ nmol cm}^{-3} \text{ d}^{-1}$ below 8 cm depth) with some intermediate peaks. One exception was 20-cm-N, where sulfate reduction peaked with an average maximum of $36 \text{ nmol cm}^{-3} \text{ d}^{-1}$ at 6–7 cm depth. Areal sulfate reduction rates integrated over the top 10 were similar for all three distances ranging between 1.4 and $1.8 \text{ mmol m}^{-2} \text{ d}^{-1}$ (Table 1).

Ammonium concentrations (0–12 cm) were generally $< 5 \mu\text{M}$ at the top of the cores and increased with depth indicating organic matter degradation (Fig. 2e). It should be mentioned that the maximum sampling depth of porewater extractions at 0-cm-N was only 5 cm, i.e. no information on ammonium concentrations at greater depths is included in the 2-D-plot at this distance. Highest values around $40 \mu\text{M}$ were reached at 20-cm-N between 7 and 11 cm. Since sulfate reduction revealed a maximum just above this layer (Fig. 2f) both peaks could be a result of sulfate reduction coupled to organic matter degradation.

Oxygen, sulfide, sulfate, porosity, and permeability were not plotted as 2D-contour maps, because they revealed little or no variability and will be described in the text only. Oxygen penetration was $\sim 3 \text{ mm}$ at 0-, 20-, and 40-cm-N. At 60-cm-N, oxygen penetration reached a maximum of 14 mm. The deeper penetration was confirmed by several replicate measurements at different positions in the same core. Oxygen concentrations in the bottom water varied between 170 and $210 \mu\text{M}$ in the cores (see above). Sulfate revealed nearly no changes with depth with respect to seawater concentration ($\sim 28 \text{ mM}$) at all distances from the vent (max. sampling depth 12 cm). No free sulfide was detected by microsensor measurements in cores from all distances (max. measured depth 5 cm). Porosity generally ranged between 0.25 and 0.35 with no clear trends (max. sampling depth 10 cm). Permeability was stable around $7 \times 10^{-12} \text{ m}^2$ at all sampled depths between 20- and 60-cm-N. The only exception was 0-cm-N, where permeability revealed a zigzag profile with values ranging between 8×10^{-11} and $7 \times 10^{-12} \text{ m}^2$ between 0 and 7 cm depth.

In summary, methane concentrations and $\delta^{13}\text{C}$ -values of methane point to anaer-

obic oxidation of methane in deeper layers of the sediments, although methane consumption (except for the 9–11 cm layer at 60-cm-N) was detected mainly at the surface (0–1 cm), where it was most likely coupled to aerobic oxidation of methane concluded from the presence of oxygen in this layer. The majority of sulfate reduction seemed not to be coupled to AOM but rather to organic matter degradation.

3.3 June sampling, Vent A and B

At Vent A, oxygen penetrated 2.2 mm with a bottom water concentration of 200 μM (Fig. 3a) compared to only 160 μM at Vent B (Fig. 3i). Here again the lower concentration at Vent B might be explained by the processing order (see above). Sulfate concentrations revealed little change with depth still reaching values of 24 mM at 10 cm depth (Fig. 3b). Ammonium concentrations fluctuated slightly but overall increased with depth to maximum values of 15–20 μM (Fig. 3c). Methane concentrations slightly increased with depth in ex-situ cores (max. 0.28 mM, Fig. 3f). The trend was less pronounced in MOX cores (values \sim 0.1 mM, Fig. 3f). Methane isotopic signatures showed depletion of the lighter carbon isotope with depth ($\delta^{13}\text{C}$ value -55.5% on top and -41.1% at the bottom, Fig. 3e) pointing to methane oxidation at depth. However, MOX rates measured to a max. depth of 14 cm revealed peak activity ($45 \text{ nmol cm}^{-3} \text{ d}^{-1}$) mainly at the surface and decreased to values $<5 \text{ nmol cm}^{-3} \text{ d}^{-1}$ below 4 cm depth (Fig. 3g). Sulfate reduction rates remained relatively stable over depth with only a slight decrease from the surface ($\sim 50 \text{ nmol cm}^{-3} \text{ d}^{-1}$) to the bottom of the cores ($\sim 20 \text{ nmol cm}^{-3} \text{ d}^{-1}$, Fig. 3h). No sulfide was detected in the measured depths (0–6 cm, Fig. 3d). Porosity and permeability revealed no clear trend with values around 0.40 and 10^{-11} m^2 , respectively (data not shown).

At Vent B, oxygen penetrated 1.4 mm (Fig. 3i). Porewater sulfate profiles were incomplete, due to problems with the pore water extraction; however, values remained at 25 mM (V-b-J) at 7 cm depth (Fig. 3j). Ammonium profiles were also incomplete and trends are difficult to identify. Generally, lower concentrations (3–7 μM) were observed at the sediment-water interface, compared to depth (18 and 51 μM at 4–5 and 6–7 cm,

Methane oxidation in permeable sediments at hydrocarbon seeps

T. Treude and W. Ziebis

Title Page

Abstract

Introduction

Conclusions

References

Tables

Figures

◀

▶

◀

▶

Back

Close

Full Screen / Esc

Printer-friendly Version

Interactive Discussion



Methane oxidation in permeable sediments at hydrocarbon seeps

T. Treude and W. Ziebis

Title Page

Abstract

Introduction

Conclusions

References

Tables

Figures

◀

▶

◀

▶

Back

Close

Full Screen / Esc

Printer-friendly Version

Interactive Discussion



respectively, Fig. 3k). Sulfide concentrations below the top cm increased linearly with depth, reaching maximum values of 2 mM between 6 and 8 cm depth (Fig. 3l). Methane concentrations increased with depth to max values of 0.42 mM (Fig. 3n). In cores sampled immediately after core retrieval (ex-situ) methane reached up to 4 times higher levels compared to MOX cores (measured 24 h after incubation). Differences could be attributed either to sediment heterogeneity or methane consumption during incubation. $\delta^{13}\text{C}$ -values of methane revealed -37% at the top and slightly decreased to -42% at the bottom of the short core (5 cm, Fig. 3m), indicating methane oxidation at the sediment surface. MOX and sulfate reduction rates basically revealed the same profile as Vent A besides that in one of each replicates a single maximum of $126 \text{ nmol cm}^{-3} \text{ d}^{-1}$ (5–6 cm) and $352 \text{ nmol cm}^{-3} \text{ d}^{-1}$ (6–7 cm) was found, respectively, pointing to elevated AOM activity (Fig. 3o and p, respectively). The two peaks were in good agreement with high sulfide levels $\sim 2.2 \text{ mM}$ detected between 6.2 and 8 cm (Fig. 3l). Porosity and permeability values were similar to Vent A (see above).

In summary, sediments taken in the vicinity of focused gas vents were dominated by subsurface activity of MOX, which, however, did not result in a depletion of sulfate. Single deeper peaks of MOX pointed to more activity of AOM at depth, which is again supported by the undersaturated methane concentrations in the porewater of the top sediment layers (see above). Areal MOX rates integrated over 10 cm depth were 1.28 and $2.38 \text{ mmol m}^{-2} \text{ d}^{-1}$ for Vent A and Vent B, respectively (Table 1). Areal sulfate reduction rates integrated over 10 cm depth were 2.30 and $3.60 \text{ mmol m}^{-2} \text{ d}^{-1}$, respectively (Table 1), i.e. by a factor of 1.8 and 1.5 higher than integrated MOX rates, respectively.

3.4 Fluorescence in situ hybridization of ANME organisms

By using fluorescently labeled oligonucleotide probes targeting specifically the ANME-1, -2, or -3, groups, only the ANME-2 probes revealed positive labeling results. Small cell aggregates of ANME-2 were found in selected samples of the 400-cm-A sediment (Fig. 4a, c). DAPI counter-staining, revealed a higher amount of total cells (Fig. 4b, d),

suggesting that the aggregates contained also other cells than ANME-2. Aggregates were not found in the top 0–2 cm of the cores (Fig. 4e). Deeper samples reached numbers of $2.3 (\pm 12 \text{ S.D.})$ and $7.3 (\pm 18 \text{ S.D.}) \times 10^6$ aggregates cm^{-3} sediment at 6–7 and 8–9 cm, respectively. Assuming that both, the aggregates and cells had a spherical shape with an average diameter of 2 and $0.5 \mu\text{m}$, respectively, and assuming a face centered cubic or hexagonal packing of the cells inside the aggregates (packing density=0.7405), aggregates had an average number of 63 cells (volume aggregate/volume cell · packing density). Accordingly, total cell numbers (including ANME-2 and additional cells in the aggregates) were approximately 1.5 and 4.6×10^8 cells cm^{-3} sediment at 6–7 and 8–9 cm depth, respectively.

4 Discussion

4.1 Methane seepage and microbial consumption in the permeable sands of Brian Seep

The shallow (~ 10 m) Brian Seep area off Coal Oil Point is characterized by a 15–20 cm thick sediment cover, which consists of well-sorted sand. Such sandy seabeds are typical for a shallow-water environment, where wave and tidal action move and resuspend the upper sediment layers (Precht et al., 2004). Coastal sands are characterized by a lower porosity compared to deep-sea muds but have a higher permeability, therefore allowing easier fluid transport through the sediment matrix. Advective transport processes, induced by pressure gradients at the sediment-water interface have been shown to transport fluids and particles much deeper and faster within permeable seabeds than is possible by diffusion (Huettel et al., 1998, 2003; Ziebis et al., 1996b). In addition, fluid and gas seepage through a permeable sediment layer can induce a convection of pore water in the surrounding sediment (Dando et al., 1994; O'Hara et al., 1995), which allows deeper penetration of oxidants in the “recharge” zone and a faster removal of reduced compounds. The gas ebullition can also strip other gases like H_2S

BGD

7, 1905–1933, 2010

Methane oxidation in permeable sediments at hydrocarbon seeps

T. Treude and W. Ziebis

Title Page

Abstract

Introduction

Conclusions

References

Tables

Figures

◀

▶

◀

▶

Back

Close

Full Screen / Esc

Printer-friendly Version

Interactive Discussion



from the pore water (O'Hara et al., 1995). Here we measured a variety of biogeochemical parameters in the sandy surface sediment (0–15 cm) of Brian Seep around sites of focused gas venting. Our primary goal was to investigate how the venting affects transport processes, geochemical gradients, and microbial methanotrophy within the permeable seabed. We carried out detailed studies along radial transects away from the seep source as well as direct measurements close to focused gas conduits. We also aimed to compare and contrast our results to methane seep environments found in deeper areas such as Hydrate Ridge (North-East Pacific, off Oregon) (Boetius and Suess, 2004; Treude et al., 2003), Gulf of Mexico (Joye et al., 2004; Orcutt et al., 2005) and the Håkon Mosby Mud Volcano (Barents Sea) (Niemann et al., 2006) (Table 2).

Sediment porosity and the permeability at Brian Seep were typical for a sandy seabed with values ranging between 0.26 and 0.45 as well as between 7×10^{-12} and $7 \times 10^{-11} \text{ m}^2$, respectively (Huettel et al., 1996). We observed a relatively deep oxygen penetration of up to 14 mm in comparison to methane seeps with less permeable fine-grained sediments (Table 2), although we want to caution that measurements in our study might not fully represent the in-situ conditions (Berg et al., 2003). Especially during times of storage and ex-situ profiling oxygen is being consumed, which results in an underestimation of oxygen concentration and penetration within the cores. Yet, the sometimes straight profile of oxygen penetration observed in Brian Seep cores suggests transport processes other than diffusion (advection, convection). Deep oxygen penetration offers an ample habitat for aerobic methanotrophs in the surface sediments of Brian Seep. In addition, waves and bottom water currents interacting with bottom topographies (e.g. ripples) induce pressure gradients in the upper permeable sediment layer, most likely leading to a frequent much deeper penetration of oxygen by pore water advection (Ziebis et al., 1996b). Even though methane turnover rate measurements using ^{14}C -labeled methane do not decipher the process responsible for methane consumption, pronounced methane turnover in the 0–1 cm layer of many sediment cores (Figs. 1h, 2d and 3g, o) suggests that aerobic rather than anaerobic methanotrophy is taking place within this interface layer. Accordingly, cells belonging to the anaerobic

BGD

7, 1905–1933, 2010

Methane oxidation in permeable sediments at hydrocarbon seeps

T. Treude and W. Ziebis

Title Page

Abstract

Introduction

Conclusions

References

Tables

Figures

◀

▶

◀

▶

Back

Close

Full Screen / Esc

Printer-friendly Version

Interactive Discussion



methanotroph (ANME) clusters were not detected in the top two centimeters (Fig. 4e). Hence, ANME communities might be excluded from this dynamic interface environment (Treude et al., 2005b). Moreover, several findings in our study indicate that the hot spot of anaerobic oxidation of methane (AOM) must be located below our sampling depth.

5 Most notable is that sulfate, the electron acceptor for AOM, remained basically unchanged (25–28 mM) with respect to seawater levels in the top 15 cm of the sediment. Sulfide, a product of AOM, was either absent or reached maximum values of 2.7 mM – a value that is about one order of magnitude lower compared to maxima reached at deep-sea seeps (Table 2). Furthermore, methane concentrations were always under-
10 saturated but often revealed increasing heavier carbon isotopic signatures with depth. Areal AOM activity in the top 10 cm was relatively low compared to deep-sea seep sites (0.6–8.7 mmol m⁻² d⁻², Table 2). ANME-2 cells, which were absent at the sediment-water interface, revealed abundances of 10⁷ to 10⁸ cells per cm³ in deeper sediment layers (6–7 and 8–9 cm). The numbers are at the lower end of advective seeps sites
15 (>10¹⁰ cells cm⁻³) and intermediate with respect to methane-rich sediments in general (min. ~10⁶ cells cm⁻³, Knittel and Boetius, 2009). Together all these point to a deep maximum of AOM, which differs from fine-grained deep-sea seep sediments. In deep-sea seep environments AOM usually reaches its maximum within the top 10 cm of the sediment, where it depletes sulfate values down to 0–5 mM simultaneously producing
20 sulfide levels of up to 26 mM (Table 2). Our findings agree well with observations from other permeable gas vent sites such as the Tommeliten area in the North Sea (North Sea, Niemann et al., 2005). At Tommeliten, sulfate levels were found to remain stable within the upper sand burden (~1.70 m thickness) but were eventually consumed by AOM in a distinct zone between silt/clay and marl sediment (between 1.70 and
25 2.50 m depth). Highest AOM activity was situated below a layer of methane-derived authigenic carbonates. Likewise, methane-derived authigenic carbonates were found below the sand burden at Brian Seeps (Kinnaman et al., 2010). Kinnaman et al. (2010) suggested that the seasonal removal of the sand burden by storms and waves during winter time periodically shifts main AOM activity into deeper sediment layers, because

Methane oxidation in permeable sediments at hydrocarbon seeps

T. Treude and W. Ziebis

Title Page

Abstract

Introduction

Conclusions

References

Tables

Figures

◀

▶

◀

▶

Back

Close

Full Screen / Esc

Printer-friendly Version

Interactive Discussion



oxygen inhibits AOM. In our study we suggest that the majority of the AOM community is permanently situated below the sand-gravel interface. Based on our observations conditions should be optimum at depth, because methane and sulfate concentrations are expected to be relatively high, the sediment is permanently anoxic, and potentially inhibiting end-products (e.g. hydrogen sulfide) would be quickly removed by convection. However, during calm periods (late spring through early autumn), AOM could partially re-establish into the upper sand layer, as suggested by the presence of ANME-2 organisms (Fig. 4e). ANME organisms are generally known for their very slow growth with doubling times of 4–7 months, which is explained by the poor energy output of AOM (Nauhaus et al., 2007). A re-establishment of the community into the upper sand layers by growth is therefore rather unlikely over such short time periods. In theory the convective pore water transport and even the uprising of gas bubbles (Schaefer et al., 1998) may serve as a means of transport for microorganisms, which might facilitate their distribution within the sediment and subsequent fast re-establishment in calm periods.

In summary, our results suggest that high permeability together with gas venting in the sediments of Brian Seep enable a fast supply of substrates (sulfate, oxygen) and corresponding removal of degradation end products (hydrogen sulfide, HCO_3^- , CO_2) that are consumed respectively produced during microbial methane oxidation (aerobic and anaerobic). The investigated dynamic surface habitat appears to be better suited for aerobic methanotrophs whereas AOM is suspected to develop its full capacity at larger depth.

4.2 ANME-2 aggregates

DAPI counter staining of fluorescently labeled ANME-2 cell aggregates (Fig. 4b, d) revealed higher cell numbers than were visible by CARD-FISH staining only (Fig. 4a, c), suggesting that the archaea form a consortium with other microorganisms at Brian Seeps. Common candidates are sulfate-reducing bacteria of the *Desulfococcus/Desulfosarcina* cluster. This group has been found most often associated with

BGD

7, 1905–1933, 2010

Methane oxidation in permeable sediments at hydrocarbon seeps

T. Treude and W. Ziebis

Title Page

Abstract

Introduction

Conclusions

References

Tables

Figures

◀

▶

◀

▶

Back

Close

Full Screen / Esc

Printer-friendly Version

Interactive Discussion



ANME-2 cells (Knittel and Boetius, 2009; Knittel et al., 2005). Other groups of Alpha-, Beta- and Deltaproteobacteria are also feasible (Knittel and Boetius, 2009 and references therein). In most cases, areal sulfate reduction rates reached similar or higher values than AOM (Table 1), suggesting that sulfate reduction was coupled to both, methanotrophy and organic matter degradation (Nauhaus et al., 2002; Treude et al., 2005b).

4.3 Suggestions for further studies

Our studies provided good indications that focused methane gas seepage through the permeable seabeds of Brian Seep induces convective porewater transport mechanisms within the surface sediment layers, which affect biogeochemical processes of methane oxidation. Yet our results are preliminary and several questions need to be solved for a full evaluation of methane turnover, consumption and flux to the water column for the permeable sediments of Brian Seep. Future investigation should focus on determining how deep the bubble-driven convective transport is reaching into the seabed and how fast solutes are turned over. An effort should be made to sample below the sediment coverage into the more coarse gravel bed to find the maximum depth of sulfate penetration, which should correspond with the hot spot of AOM activity. Such an undertaking can probably only be achieved by the application of robust sampling techniques such as vibro-coring with the disadvantage of porewater disturbances during sampling. However, only if we understand the full capacity of AOM activity within these near-shore habitats we will be able to include them in calculations of local and global methane budgets.

Acknowledgements. We greatly thank D. Valentine and F. Kinnaman from UCSB for logistical support during joint field trips to Brian Seep and for data discussions. We also acknowledge D. Farrar, S. Anderson, and E. Hessel from UCSB for support during SCUBA dives. K. Stange and B. Domeyer from IFM-GEOMAR are thanked for measuring $\delta^{13}\text{C}$ -values of methane and sulfate concentrations, respectively. This work was funded by the University of Southern California (USC) and the German Research Foundation (DFG, Fellowship No. Tr 867/1-1).

BGD

7, 1905–1933, 2010

Methane oxidation in permeable sediments at hydrocarbon seeps

T. Treude and W. Ziebis

Title Page

Abstract

Introduction

Conclusions

References

Tables

Figures

◀

▶

◀

▶

Back

Close

Full Screen / Esc

Printer-friendly Version

Interactive Discussion



References

- Allen, A. A. and Mikolaj, P. G.: Natural oil seepage at Coal Oil Point, Santa Barbara, California, *Science*, 170, 974–980, 1970.
- 5 Berg, P., Røy, H., Janssen, F., Meyer, V., Jørgensen, B. B., Huettel, M., and De Beer, D.: Oxygen uptake by aquatic sediments measured with a novel non-invasive eddy-correlation technique, *Mar. Ecol. Prog. Ser.*, 261, 75–83, 2003.
- Boetius, A., Ravensschlag, K., Schubert, C. J., Rickert, D., Widdel, F., Giesecke, A., Amann, R., Jørgensen, B. B., Witte, U., and Pfannkuche, O.: A marine microbial consortium apparently mediating anaerobic oxidation of methane, *Nature*, 407, 623–626, 2000.
- 10 Boetius, A. and Suess, E.: Hydrate Ridge: A natural laboratory for the study of microbial life fueled by methane from near-surface gas hydrates, *Chem. Geol.*, 205, 291–310, 2004.
- Boles, J. R. and Clark, J. F.: Temporal variation in natural methane seep rate due to tides, Coal Oil Point area, California, *J. Geophys. Res.*, 106, 27077–27086, 2001.
- Cline, J. D.: Spectrophotometric determination of hydrogen sulfide in natural waters, *Limnol. Oceanogr.*, 14, 454–458, 1969.
- 15 Dando, P. R., O'Hara, S. C. M., Schuster, U., Taylor, L. J., Clayton, C. J., Baylis, S., and Laier, T.: Gas seepage from carbonate-cemented sandstone reef on the Kattegat coast of Denmark, *Mar. Petr. Geol.*, 11, 182–189, 1994.
- Hall, P. O. J. and Aller, R. C.: Rapid small-volume flow injection analysis for ΣCO_2 and NH_4^+ in marine and fresh waters, *Limnol. Oceanogr.*, 37, 1113–1119, 1992.
- 20 Hornafius, J. S., Quigley, D., and Luyendyk, B. P.: The world's most spectacular marine hydrocarbon seeps (Coal Oil Point, Santa Barbara Channel, California): quantification of emissions, *J. Geophys. Res.*, 104, 20703–20711, 1999.
- Huettel, M., Ziebis, W., and Forster, S.: Flow-induced uptake of particulate matter in permeable sediments, *Limnol. Oceanogr.*, 41, 309–322, 1996.
- 25 Huettel, M., Ziebis, W., Forster, S., and Luther, I. G. W.: Advective transport affecting metal and nutrient distribution and interfacial fluxes in permeable sediments, *Geochim. Cosmochim. Acta*, 62, 613–631, 1998.
- Huettel, M., Røy, H., Precht, E., and Ehrenhaus, S.: Hydrodynamical impact on biogeochemical processes in aquatic sediments, *Hydrobiologia*, 494, 231–236, 2003.
- 30 Jeroschewsky, P., Steuckart, C., and Kuehl, M.: An amperometric microsensor for the determination of H_2S in aquatic environments, *Anal. Chem.*, 68, 4351–4357, 1996.

BGD

7, 1905–1933, 2010

Methane oxidation in permeable sediments at hydrocarbon seeps

T. Treude and W. Ziebis

Title Page

Abstract

Introduction

Conclusions

References

Tables

Figures

◀

▶

◀

▶

Back

Close

Full Screen / Esc

Printer-friendly Version

Interactive Discussion



Methane oxidation in permeable sediments at hydrocarbon seeps

T. Treude and W. Ziebis

Title Page

Abstract

Introduction

Conclusions

References

Tables

Figures

◀

▶

◀

▶

Back

Close

Full Screen / Esc

Printer-friendly Version

Interactive Discussion



Jørgensen, B. B.: A comparison of methods for the quantification of bacterial sulphate reduction in coastal marine sediments: I. Measurements with radiotracer techniques, *Geomicrobiol. J.*, 1, 11–27, 1978.

Joye, S. B., Boetius, A., Orcutt, B. N., Montoya, J. P., Schulz, H. N., Erickson, M. J., and Logo, S. K.: The anaerobic oxidation of methane and sulfate reduction in sediments from Gulf of Mexico cold seeps, *Chem. Geol.*, 205, 219–238, 2004.

Kallmeyer, J., Ferdelman, T. G., Weber, A., Fossing, H., and Jørgensen, B. B.: A cold chromium distillation procedure for radiolabeled sulfide applied to sulfate reduction measurements, *Limnol. Oceanogr. Methods*, 2, 171–180, 2004.

Kinnaman, F. S., Valentine, D. L., and Tyler, P. A.: Carbon and hydrogen isotope fractionation associated with the aerobic microbial oxidation of methane, ethane, propane and butane, *Geochim. Cosmochim. Acta*, 71, 271–283, 2007.

Kinnaman, F. S., Kimball, J. B., Busso, L., Birgel, D., Ding, H., Hinrichs, K.-U., and Valentine, D. L.: Gas flux and carbonate occurrence at a shallow seep of thermogenic natural gas, *Geo-Mar. Lett.*, doi:10.1007/s00367-010-0184-0, in press, 2010

Knittel, K., Lösekann, T., Boetius, A., Kort, R., and Amann, R.: Diversity and distribution of methanotrophic Archaea (ANME) at cold seeps, *Appl. Environ. Microbiol.*, 71, 467–479, 2005.

Knittel, K. and Boetius, A.: Anaerobic oxidation of methane: progress with an unknown process, *Annu. Rev. Microbiol.*, 63, 311–334, 2009.

Krumbein, W. C. and Monk, G. D.: Permeability as a function of the size parameters of unconsolidated sand, *Trans. Am. Inst. Min. Metall. Petr. Eng.*, 151, 153–163, 1943.

Kühl, M., Steuckart, C., Eickert, G., and Jeroschewsky, P.: A H₂S microsensor for profiling biofilms and sediments: application in an acidic lake sediment, *Aquat. Microb. Ecol.*, 15, 201–209, 1998.

Mau, S., Valentine, D. L., Clark, J. F., Reed, J., and Camilli, R.: Dissolved methane distribution and air-sea flux in the plume of a massive seep field, Coal Oil Point, California, *Geophys. Res. Lett.*, 34, L22603, doi:10.1029/2007GL031344, 2007.

Nauhaus, K., Boetius, A., Krüger, M., and Widdel, F.: In vitro demonstration of anaerobic oxidation of methane coupled to sulphate reduction in sediment from marine gas hydrate area, *Environ. Microbiol.*, 4, 298–305, 2002.

Nauhaus, K., Albrecht, M., Elvert, M., Boetius, A., and Widdel, F.: In vitro cell growth of marine archaeal-bacterial consortia during anaerobic oxidation of methane with sulfate, *Environ. Microbiol.*, 9, 187–196, 2007.

Niemann, H., Elvert, M., Hovland, M., Orcutt, B., Judd, A., Suck, I., Gutt, J., Joye, S., Damm, E., Finster, K., and Boetius, A.: Methane emission and consumption at a North Sea gas seep (Tommeliten area), *Biogeosciences*, 2, 335–351, 2005, <http://www.biogeosciences.net/2/335/2005/>.

5 Niemann, H., Lösekann, T., De Beer, D., Elvert, M., Nadalig, T., Knittel, K., Aman, A., Sauter, E. J., Schlüter, M., Klages, M., Foucher, J.-P., and Boetius, A.: Novel microbial communities of the Haakon Mosby mud volcano and their role as a methane sink, *Nature*, 443, 854–858, 2006.

O'Hara, S. C. M., Dando, P. R., Schuster, U., Bennis, A., Boyle, J. D., Chui, F. T. W., Hatherell, T. V. J., Niven, S. J., and Yalor, L. J.: Gas seep induced interstitial water circulation: observations and environmental implications, *Cont. Shelf Res.*, 15, 931–948, 1995.

Orcutt, B. N., Samarkin, V., Boetius, A., and Joye, S. B.: On the relationship between methane production and oxidation by anaerobic methanotrophic communities from cold seep of the Gulf of Mexico, *Environ. Microbiol.*, 10, 1108–1117, 2008.

15 Orcutt, E., Boetius, A., Elvert, M., Samarkin, V., and Joye, S. B.: Molecular biogeochemistry of sulfate reduction, methanogenesis and anaerobic oxidation of methane at Gulf of Mexico cold seeps, *Geochim. Cosmochim. Acta*, 69, 4267–4281, 2005.

Precht, E., Franke, U., Polerecky, L., and Huettel, M.: Oxygen dynamics in permeable sediments with wave-driven pore water exchange, *Limnol. Oceanogr.*, 49, 693–705, 2004.

20 Revsbech, N. P.: An oxygen microelectrode with a guard cathode, *Limnol. Oceanogr.*, 34, 474–478, 1989.

Rice, A. L., Gotoh, A. A., Ajie, H. O., and Tyler, S. C.: High-precision continuous-flow measurements of $\delta^{13}\text{C}$ and δD of atmospheric CH_4 , *Anal. Chem.*, 73, 4104–4110, 2001.

25 Sahling, H., Rickert, D., Raymond, W. L., Linke, P., and Suess, E.: Macrofaunal community structure and sulfide flux at gas hydrate deposits from the Cascadia convergent margin, NE Pacific, *Mar. Ecol. Prog. Ser.*, 231, 121–138, 2002.

Schaefer, A., Harms, H., and Zehnder, A. D. J.: Bacterial accumulation at the air-water interface, *Environ. Sci. Technol.*, 32, 3704–3712, 1998.

30 Snaidr, J., Amann, R., Huber, I., Ludwig, W., and Schleifer, K. H.: Phylogenetic analysis and in situ identification of bacteria in activated sludge, *Appl. Environ. Microbiol.*, 65, 3976–3981, 1997.

Soltwedel, T., Portnova, D., Kolar, I., Mokievsky, V., and Schewe, I.: The small-sized benthic biota of the Haakon Mosby Mud Volcano (SW Barents Sea slope), *J. Mar. Systems*, 55,

BGD

7, 1905–1933, 2010

Methane oxidation in permeable sediments at hydrocarbon seeps

T. Treude and W. Ziebis

Title Page

Abstract

Introduction

Conclusions

References

Tables

Figures

◀

▶

◀

▶

Back

Close

Full Screen / Esc

Printer-friendly Version

Interactive Discussion



271–290, 2005.

Sommer, S., Pfannkuche, O., Linke, P., Luff, R., Greinert, J., Drews, M., Gubsch, S., Pieper, M., Poser, M., and Viergutz, T.: Efficiency of the benthic filter: Biological control of the emission of dissolved methane from sediments containing shallow gas hydrates at Hydrate Ridge, Global Biogeochem. Cy., 20, 1–14, 2006.

Sommer, S., Linke, P., Pfannkuche, O., Niemann, H., and Treude, T.: Benthic respiration in a seep habitat dominated by dense beds of ampharetid polychaetes at the Hikurangi Margin (New Zealand), Mar. Geol., doi:10.1016/j.margeo.2009.1006.1003, in press, 2010.

Treude, T.: Anaerobic oxidation of methane in marine sediments, Fachbereich Biologie/Chemie, Universität Bremen, 245, online available at: http://elib.suub.uni-bremen.de/publications/dissertations/E-Diss845_treude.pdf, 2003.

Treude, T., Boetius, A., Knittel, K., Wallmann, K., and Jørgensen, B. B.: Anaerobic oxidation of methane above gas hydrates at Hydrate Ridge, NE Pacific Ocean, Mar. Ecol. Prog. Ser., 264, 1–14, 2003.

Treude, T., Knittel, K., Blumenberg, M., Seifert, R., and Boetius, A.: Subsurface microbial methanotrophic mats in the Black Sea, Appl. Environ. Microbiol., 71, 6375–6378, 2005a.

Treude, T., Krüger, M., Boetius, A., and Jørgensen, B. B.: Environmental control on anaerobic oxidation of methane in the gassy sediments of Eckernförde Bay (German Baltic), Limnol. Oceanogr., 50, 1771–1786, 2005b.

Yamamoto, S., Alcauskas, J. B., and Crozier, T. E.: Solubility of methane in distilled water and seawater, J. Chem. Eng. Data, 21, 78–80, 1976.

Ziebis, W., Huettel, M., and Forster, S.: The impact of biogenic sediment topography on oxygen fluxes in permeable sediments, Mar. Ecol. Prog. Ser., 140, 227–237, 1996b.

BGD

7, 1905–1933, 2010

Methane oxidation in permeable sediments at hydrocarbon seeps

T. Treude and W. Ziebis

Title Page

Abstract

Introduction

Conclusions

References

Tables

Figures

◀

▶

◀

▶

Back

Close

Full Screen / Esc

Printer-friendly Version

Interactive Discussion



Methane oxidation in permeable sediments at hydrocarbon seeps

T. Treude and W. Ziebis

Table 1. Areal rates of methane oxidation and sulfate reduction. Replicates were averaged ($n = 2-4$) and integrated over 10 cm sediment depth. n.d.=not determined.

	Methan oxidation $\text{mmol m}^{-2} \text{d}^{-1}$	Sulfate reduction $\text{mmol m}^{-2} \text{d}^{-1}$
April		
20 cm	2.97	n.d.
200 cm	7.79	1.67
400 cm	8.69	4.08
June		
Vent A	1.28	2.30
Vent B	2.38	3.60
November		
0 cm	1.34	1.46
20 cm	0.91	1.76
40 cm	1.08	1.41
60 cm	0.61	1.48

Title Page

Abstract

Introduction

Conclusions

References

Tables

Figures

◀

▶

◀

▶

Back

Close

Full Screen / Esc

Printer-friendly Version

Interactive Discussion



Methane oxidation in permeable sediments at hydrocarbon seeps

T. Treude and W. Ziebis

Table 2. Comparison of biogeochemical parameters between Bryan seep (shallow sandy sediment) and deep-sea seeps (fine-grained muddy sediments). Considered are sites revealing the highest AOM rates and not containing bioturbation/bioirrigation activity of clams or annelid worms. PD=penetration depth; mM at cm=concentration measured at max sampling depth or where sulfate reached zero; Max [CH₄]=maximum methane concentration measured in the top 15 cm of the sediment at atmospheric pressure; Max [H₂S]=maximum sulfide concentration measured in the top 15 cm of the sediment; MOX=methane oxidation (aerobic and anaerobic) integrated over 10 cm sediment depth; n.d.=not determined. Sources: 1=Boetius and Suess, 2004; Sahling et al., 2002; Sommer et al., 2006; Treude et al., 2003; Treude et al., unpubl. data; 2=Joye et al., 2004; Orcutt et al., 2005; Orcutt et al., 2008; 3=Niemann and Loesekann, 2006; Soltwedel et al., 2005.

Cold Seep	Sediment type	Porosity	Oxygen PD (cm)	Sulfate PD (mM at cm)	Max [CH ₄] (mM)	Max [H ₂ S] (mM)	MOX rate (mmol m ² d ⁻¹)	Sources
Bryan Seep	sand	0.26–0.45	0.2–1.4	25 at 13	0.14–1.06	0–2	0.6–8.7	this study
Hydrate Ridge	fine-grained mud	0.62–0.73	0.0–0.7	2 at 10	1.0–4.2	10–26	99	1
Gulf of Mexico	fine-grained mud	0.6	n.d.	1–5 at 10	1.4–7.0	10–20	2.6–4.6	2
Håkon Mosby Mud Volcano	fine-grained mud	0.43–0.64	0.1–0.2	0 at 4–6	n.d.	5	4.5	3

Title Page

Abstract

Introduction

Conclusions

References

Tables

Figures



Back

Close

Full Screen / Esc

Printer-friendly Version

Interactive Discussion



Methane oxidation in permeable sediments at hydrocarbon seeps

T. Treude and W. Ziebis

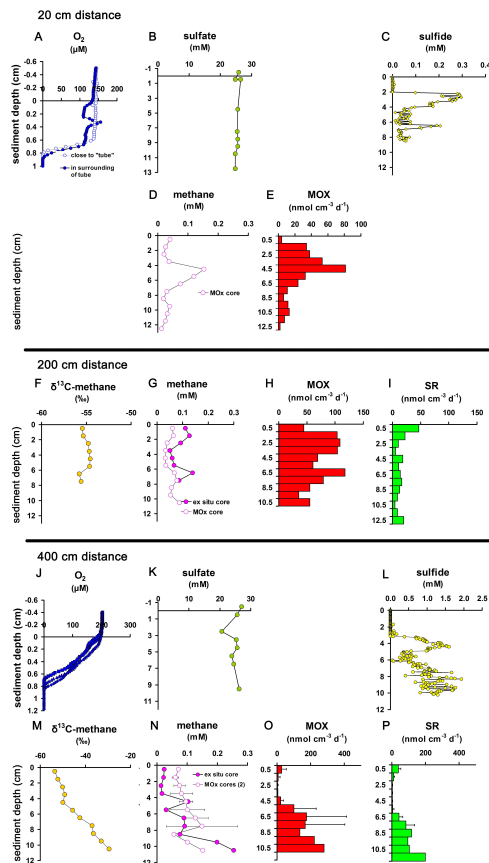


Fig. 1. Biogeochemical profiles of the April sampling at Brian Seep. Samples are available from 20, 200, and 400 cm distance from the gas vent. Oxygen profiles show up to three replicates. Methane profiles show methane concentrations of samples taken immediately after recovery (ex situ core) or after 24 h incubation (MOX core). MOX (methane oxidation) and SR (sulfate reduction rates) at 400 m distance represent the average and standard deviation of two replicates.

Title Page

Abstract

Introduction

Conclusions

References

Tables

Figures

◀

▶

◀

▶

Back

Close

Full Screen / Esc

Printer-friendly Version

Interactive Discussion



Methane oxidation in permeable sediments at hydrocarbon seeps

T. Treude and W. Ziebis

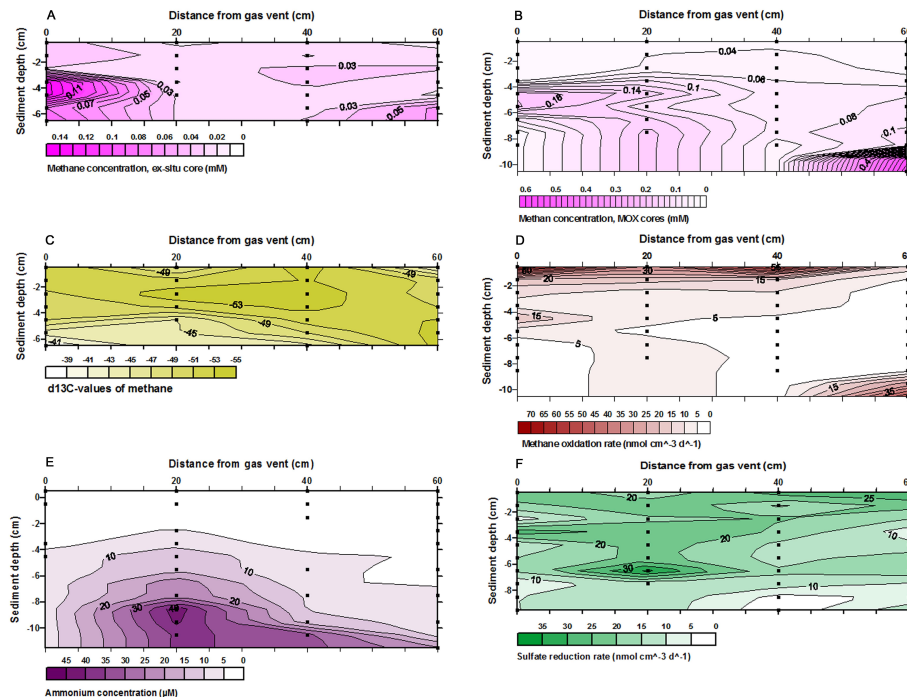


Fig. 2. 2-D-contour maps of biogeochemical profiles of the November sampling as a function of transect distance (x-axes) and sediment depth (y-axes). Samples were taken at 0, 20, 40, and 60 cm distance from a gas vent. Methane profiles show methane concentrations of samples taken immediately after recovery (ex-situ core) or after 24 h incubation (MOX core). Sampled depths are highlighted by black dots in the maps. Please consider that the maximum sampling depth for methane (MOX core), methane oxidation rates, and ammonium was not reached in all cores, i.e. contour lines at the larger depth have to be viewed with great caution.

Title Page

Abstract

Introduction

Conclusions

References

Tables

Figures

◀

▶

◀

▶

Back

Close

Full Screen / Esc

Printer-friendly Version

Interactive Discussion



Methane oxidation in permeable sediments at hydrocarbon seeps

T. Treude and W. Ziebis

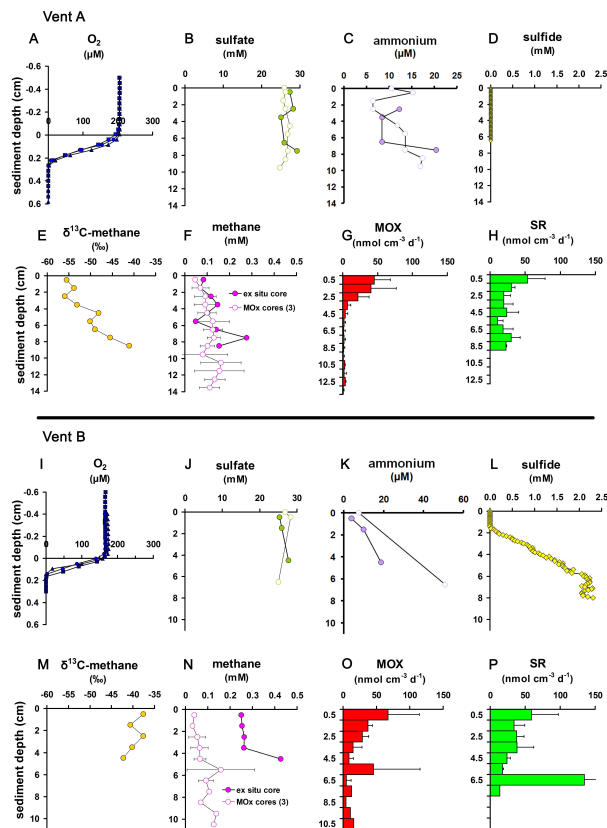


Fig. 3. Biogeochemical profiles of the June sampling at Brian Seep. Cores were sampled close to gas vents (Vent A and B). Oxygen profiles show up to three, sulfate and ammonium profiles two replicates. Methane profiles show methane concentrations of samples taken immediately after recovery (ex-situ core) or after 24hr incubation (MOX core). MOX (methane oxidation) and SR (sulfate reduction rates) represent the average and standard deviation of 3–4 replicates.

Title Page

Abstract

Introduction

Conclusions

References

Tables

Figures

◀

▶

◀

▶

Back

Close

Full Screen / Esc

Printer-friendly Version

Interactive Discussion



Methane oxidation in permeable sediments at hydrocarbon seeps

T. Treude and W. Ziebis

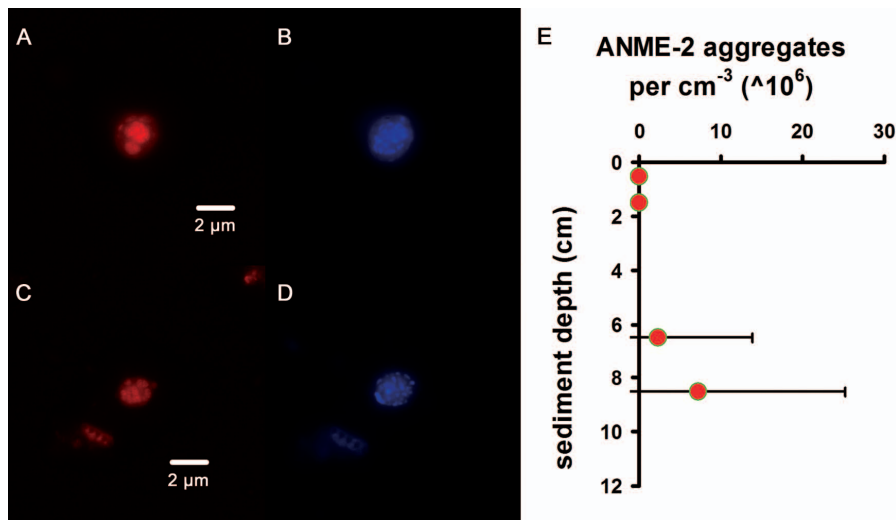


Fig. 4. (A, C) In situ identification of ANME-2 aggregates with fluorescently labeled rRNA-targeted oligonucleotide probes (ALEXA 488-labeled). (B, D) DAPI counter staining. (E) Abundance of ANME-2 aggregates in selected depths of a sediment core taken at 400-cm-A. Average aggregate size was 2 μm consisting of ~63 total cells.

Title Page

Abstract

Introduction

Conclusions

References

Tables

Figures

◀

▶

◀

▶

Back

Close

Full Screen / Esc

Printer-friendly Version

Interactive Discussion

